THE JOURNAL OF
PHYSICAL CHEMISTRY C

Article

pubs.acs.org/JPCC

Low-Temperature, Directly Depositing Individual Single-Walled Carbon Nanotubes for Fabrication of Suspended Nanotube Devices

Yuanchun Zhao,*[,†] Zheng Liu,[†] Guangtong Liu,[‡] Kaihong Zheng,[†] Lijun Hu,[†] Wenjun Ma,[‡] Yan Ren,[‡] Changzhi Gu,[‡] Sishen Xie,[‡] and Lianfeng Sun*[,†]

[†]National Center for Nanoscience and Technology, Beijing 100190, China

[‡]Beijing National Laboratory for Condensed Matter Physics and Institute of Physics, Chinese Academy of Sciences, Beijing 100190, China

Supporting Information

ABSTRACT: Single-walled carbon nanotubes (SWNTs) grown by chemical vapor deposition (CVD) are widely used for fabrication of high-performance nanotube devices. However, the high-temperature growth is incompatible with the current complementary metal-oxide semiconductor (CMOS) technology. We demonstrate a low-temperature and direct deposition of the CVD-grown SWNTs. The nanotubes are synthesized by floating catalytic CVD technique and further carried by the flowing gas directly to the low-temperature area. Individual SWNTs have been successfully deposited on Si/SiO_2 substrates covered with a polymethylmethacrylate layer, which results in a suspended geometry of the nanotube in the fabricated devices. We subsequently investigate the electrical-transport properties of a representative small band gap nanotube, which exhibits an ambipolar feature with *p*-channel mobility up to 1410 $cm^2\ V^{-1}\ S^{-1}$ at room temperature. Furthermore, low-temperature measurements down to 4 K reveal different transport characteristics with the gate voltage biased near zero or at a large negative value, respectively.

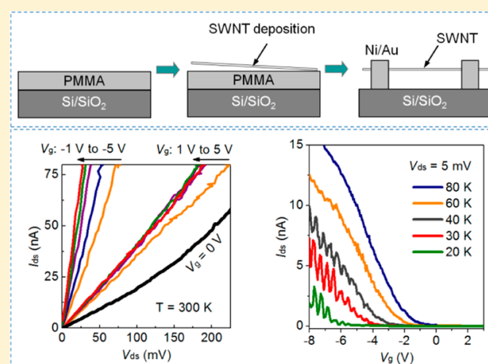

■ INTRODUCTION

The combination of exceptional electronic properties and unique 1D feature makes single-walled carbon nanotubes (SWNTs) the most promising materials for future nano-electronic applications.[1,2] Recently, field-effect transistors (FETs) based on semiconducting SWNTs have been scaled down to sub-10 nm channel length,[3] exhibiting a distinct ballistic transport and competitive performances to that of the Si-based devices at similar dimensions. SWNT FETs with large channel lengths exhibit outstanding diffusive transport characteristics with field-effect mobilities ranging from 10^3 to 10^4 $cm^2\ V^{-1}\ S^{-1}$.[4−6] Meanwhile, researchers continuously made efforts on the so-called metallic SWNTs and gained new insights into their intrinsic electronic properties,[7−9] and the small band gap caused by curvature of the nanotube could lead to unique application potentials.[10,11] Synthesis of clean and defect-free nanotubes is crucial for fabricating high-performance SWNT devices, and the high-temperature growth via chemical vapor deposition (CVD) is the most successful and widely used method to produce these high-quality nanotubes.[4,6,12−14]

SWNT devices are commonly fabricated by using the well-developed lithographic techniques, especially electron beam lithography (EBL). To improve the device performances and explore specific applications of SWNTs, multistep processes have been developed to fabricate complicated device structures, such as suspended (nanotube) channel,[9,15−18] local gates,[19,20] asymmetry contacts built with different metals,[21−23] and so on. The wet-chemistry-involved fabrication process, however, does not possess compatibility with the high-temperature growth of the SWNTs, which inhibits further improvements toward more facile and reliable fabrication of the SWNT devices, especially those with complicated structures. An attractive alternative is to disperse the synthesized SWNTs in solution, followed by nanotube-type separation and assembly, and finally deposit the wanted SWNTs on substrates for device fabrication. Recently, significant progress has been made on FETs constructed with solution-processed SWNTs by controlling the structure and cleanliness of SWNTs,[24,25] improving the design of device structure,[26−28] choosing specific materials for electrodes and dielectrics,[26,29] shrinking the channel length,[30] and so on. However, the short average length and the defects in the solution-processed SWNTs, which are induced by the intense acid treatment and aggressive sonication, are still the general and unsolvable difficulties.

In this work, we first demonstrate the low-temperature and direct deposition of CVD-grown SWNTs and then report a facile fabrication of suspended nanotube devices based on this low-temperature deposition method. SWNTs are synthesized via floating catalytic CVD technique.[31−33] The as-synthesized SWNTs are carried by the gas flow, cross the high-temperature

Received: May 30, 2013
Revised: July 14, 2013
Published: July 15, 2013

 © 2013 American Chemical Society dx.doi.org/10.1021/jp405320k | J. Phys. Chem. C 2013, 117, 16256−16262

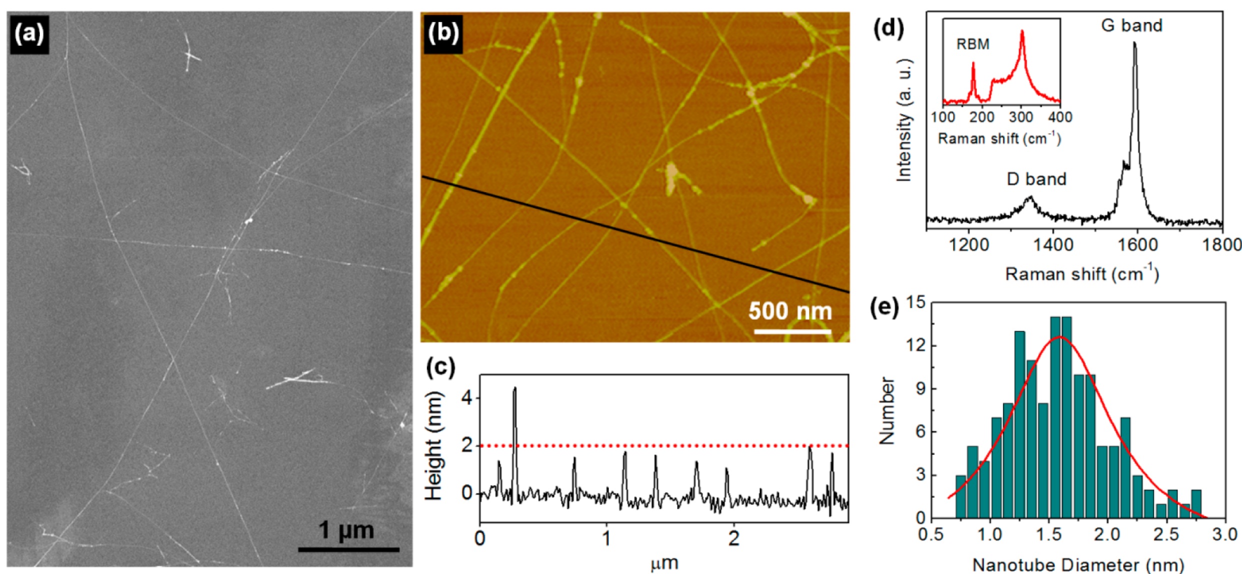

Figure 1. Direct deposition of SWNTs via floating catalytic CVD. (a) SEM image of the SWNTs deposited in low-temperature area. (b) AFM image of the as-deposited SWNTs and (c) the corresponding section analyses, revealing eight individual nanotubes with diameters from 1.3 to 2.0 nm as well as a small nanotube bundle. (d) Resonant Raman spectrum of a semiconducting SWNT. The inset shows its RBM peak at 177 cm^{-1}, corresponding to a diameter of ~1.4 nm. (e) Diameter distribution of over 130 SWNTs measured by AFM, which were collected from six different Si substrates under the optimized depositing conditions. The solid line presents a Lorentzian fit, exhibiting an average diameter of ~1.6 nm.

growth region, and deposit on substrates placed in the low-temperature area. Most of the deposited nanotubes are individual, with a typical length exceeding 10 μm. We successfully deposit individual SWNTs on Si/SiO_2 substrates covered with a polymethylmethacrylate (PMMA) layer. This simple extra step suspends the nanotubes in the fabricated devices. In the last section, we focus on the electrical characteristics of a suspended small band gap nanotube device fabricated via this approach, which reveals an ambipolar feature with peak mobilities of ~1410 $cm^2\ V^{-1}\ S^{-1}$ for hole conduction and ~120 $cm^2\ V^{-1}\ S^{-1}$ for electron conduction. This low-temperature depositing process is compatible with the current complementary metal-oxide semiconductor (CMOS) technology and thus holds the potential to be a new platform for high-performance SWNT devices. Moreover, this approach can deposit SWNTs on various substrates and surfaces, which is also attractive for nanotube-based flexible electronics and biological applications.

■ EXPERIMENTAL SECTION

Synthesis and Deposition of Individual SWNTs. Individual SWNTs were synthesized via floating catalytic CVD method, and the detailed description can be found in our previous works.[31,34] SWNT synthesis and low-temperature deposition were carried out in a quartz tube. In its beginning region, the catalyst (a mixture of ferrocene and sulfur) was sublimed at a temperature of 60−62 °C, and subsequently carried by Ar (carrying gas, 1100 sccm) and methane (2 sccm, carbon source) flow to the high-temperature growth region (1100 °C), where SWNTs continuously grew from the catalyst particles. The synthesized SWNTs were further carried by the flowing gas to the end region of the quartz tube, where the temperature sharply decreased to 60 °C. Various substrates can be loaded in this low-temperature area to directly deposit the newly synthesized SWNTs.

Fabrication of Suspended Nanotube Devices. We used *n*-doped Si wafers capped with a 200 nm-thick oxide layer as substrates. First of all, a 100-nm-thick PMMA layer was spin-coated on the Si/SiO_2 substrates. These special substrates were loaded into the low-temperature area to collect individual SWNTs. Then, a second layer of PMMA with thickness of 260 nm was added on the top of the as-deposited SWNTs to form a PMMA/SWNT/PMMA sandwich structure. In the third step, desired patterns were defined by using EBL (Raith 150). The exposed PMMA, including both the 100 and 260 nm thick layers, was developed. Finally, Ni/Au electrodes (20 nm/100 nm) were deposited via metal evaporation. After the lift-off process, devices with suspended SWNTs were fabricated.

Characterizations and Measurements. The deposited SWNTs were characterized by scanning electron microscopy (SEM, Hitachi S-5200) at 5 kV, atomic force microscopy (AFM, Nanoman II), and micro-Raman spectroscopy (Renishaw inVia Raman spectroscope) with an excitation source of a 514.5 nm laser. The fabricated devices were measured in air or loaded into an Oxford cryostat for low-temperature measurements. Electrical measurements were carried out by a Keithley 4200 semiconductor characterization system, and the heavily doped Si substrate was used as backgate.

■ RESULTS AND DISCUSSION

Floating catalytic CVD technique has been employed to synthesize high-quality SWNT thin films. The continuous, high-yield growth forms nanotube bundles due to the strong van der Waals interaction. The nanotube bundles further cross-link to form networks and finally produce mechanically strong, highly conducting, and transparent SWNT thin films.[31] To produce individual nanotubes, however, it is crucial to lower the growth rate as much as possible. In the optimized growth, the catalyst source was sublimed at a relatively low temperature ranging from 60 to 62 °C, and thus the generated catalyst particles were controlled at a proper level. Meanwhile, the carbon source (methane in this work) was adjusted to a very small flux of 2 sccm. In this case, the as-grown SWNTs were

dx.doi.org/10.1021/jp405320k | J. Phys. Chem. C 2013, 117, 16256−16262

uniformly dispersed and floated in the flowing gas and directly carried to the low-temperature area.

Another challenge is to eliminate the amorphous carbon generated in the intermediate-temperature region. SWNT thin films deposited in the high-temperature region are clean and defect-free (see Supporting Information, Figure S1). When the carrying gas (mixture of Ar and methane) flows through the intermediate-temperature region, the growth of the floated nanotubes is stopped; however, the carbon source (methane) is still decomposed to promote the formation of amorphous carbon on the deactivated catalyst particles as well as the synthesized nanotubes. This process can be suppressed by a careful control of the ratio and flux of the gas mixture (see Supporting Information, Figure S2). As far as the optimized depositing parameters are concerned, the flux of carbon source (methane) is fixed at a very small value of 2 sccm, which not only results in a low yield of the nanotube growth that produces individual SWNTs but also suppress the formation of amorphous carbon in the intermediate-temperature region. A proper flux of the carrying Ar gas (1100 sccm for the optimized deposition) also plays a key role in depositing long and clean nanotubes in the low-temperature region. Smaller flux of the carrying Ar (800−1000 sccm) produces high-quality SWNT thin films in the high-temperature region,[31] but only short nanotubes with a large amount of amorphous carbon can be carried to the low-temperature region (see Supporting Information, Figure S2). Larger flux of the flowing Ar gas carries long nanotubes to the low-temperature region, and the formation of amorphous carbon is further suppressed because the synthesized SWNTs are carried through the intermediate-temperature region at a higher speed. Figure 1a shows a SEM image of the SWNTs deposited in the low-temperature area down to 60 °C. The deposited SWNTs are long, isolated, and quite clean. The typical length of the nanotubes is longer than 10 μm, which is highly satisfied for device fabrication. Note that some of the nanotubes are still partially covered by amorphous carbon. Figure 1b shows a typical AFM image, clearly revealing that the deposited SWNTs are quite clean but with amorphous carbon partially attached. Although the nanotube density is a little higher, most of the deposited SWNTs are individual. As shown in Figure 1c, the corresponding cross-section analyses indicate eight individual nanotubes with diameters ranging from 1.3 to 2.0 nm as well as a small nanotube bundle. Furthermore, it is important to note: (i) the deposition time for these samples is as long as 10 min, and thus it is facile to control the nanotube density by simply adjusting the depositing duration; (ii) the partially postattached amorphous carbon has no effect on the pristine quality of the nanotubes; and (iii) further improvements are feasible to produce cleaner SWNTs by choosing different carbon sources, sharpening the temperature drop from growth region to deposition area, and so on.

The as-deposited nanotubes are further investigated by micro-Raman spectroscopy with a 514.5 nm excitation laser. As shown in Figure 1d, the tangential Raman modes (G band, 1500−1600 cm^{-1}) exhibit distinct features (splitting into G$^+$ and G$^-$ modes) for SWNTs, and the G$^-$ peak reveals a symmetry line shape. The inset of Figure 1d shows the radial breathing mode (RBM) at a frequency of 177 cm^{-1}, corresponding to a nanotube diameter of ∼1.4 nm. This individual SWNT is semiconducting and resonant with the incident laser (E_{laser}= 2.41 eV) with respect to its interband energy E_s.[33,35]

To obtain the average information of the diameters of the obtained SWNTs, we selected different samples (nanotubes on Si substrates) deposited at the optimal conditions to perform AFM measurements. It was found that most of the nanotubes (>90%) have diameters ranging from 0.7 to 3.0 nm. Figure 1e shows the diameter distribution of the as-deposited SWNTs, nearly 80% of the nanotubes have a diameter between 1.0 and 2.0 nm. The distribution can be well-fitted by a Lorentzian function, with an average diameter of ∼1.6 nm.

The low-temperature deposition of CVD-grown SWNTs is compatible with the current CMOS technology and also a novel method for direct deposition of SWNTs on various substrates and surfaces. With the optimized experimental parameters, the temperature in the deposition area is down to 60 °C. Most of the EBL resists, and photoresists are available for the SWNT deposition. It is facile to fabricate special patterns and structures of these resists on the required substrates before the nanotube deposition; therefore, the fabrication process of nanotube devices can be further improved. Here we choose Si/SiO_2 wafer coated with a PMMA layer as substrates and demonstrate a conventional fabrication of suspended nanotube devices based on the low-temperature SWNT deposition. As shown in Figure 2a, an individual SWNT is deposited on the PMMA surface. After the nanotube deposition, a second PMMA layer is added to form a PMMA/SWNT/PMMA sandwich structure. Then, the standard EBL and metal evaporation process are used to fabricate electrode patterns. Figure 2b shows a typical SEM image of the as-fabricated SWNT device, and the inset presents the corresponding schematic cross-sectional view. The nanotube is enclosed and fixed by the metal electrodes, which results in a suspended geometry.[34,36] The height of the suspended nanotube over the oxide layer surface is determined by the

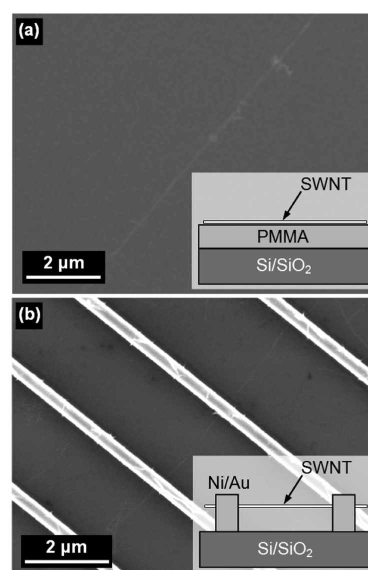

Figure 2. (a) SEM image of an individual SWNT deposited on Si/SiO_2 substrate coated with a 100 nm thick layer of PMMA. The low-temperature deposition has no effect on the PMMA layer. (b) SEM image of the as-fabricated SWNT device. The nanotube is enclosed and fixed by the electrodes and suspended over the substrate. The corresponding height is determined by the thickness of the precoated PMMA layer. The inset in each image shows the schematic cross-sectional views.

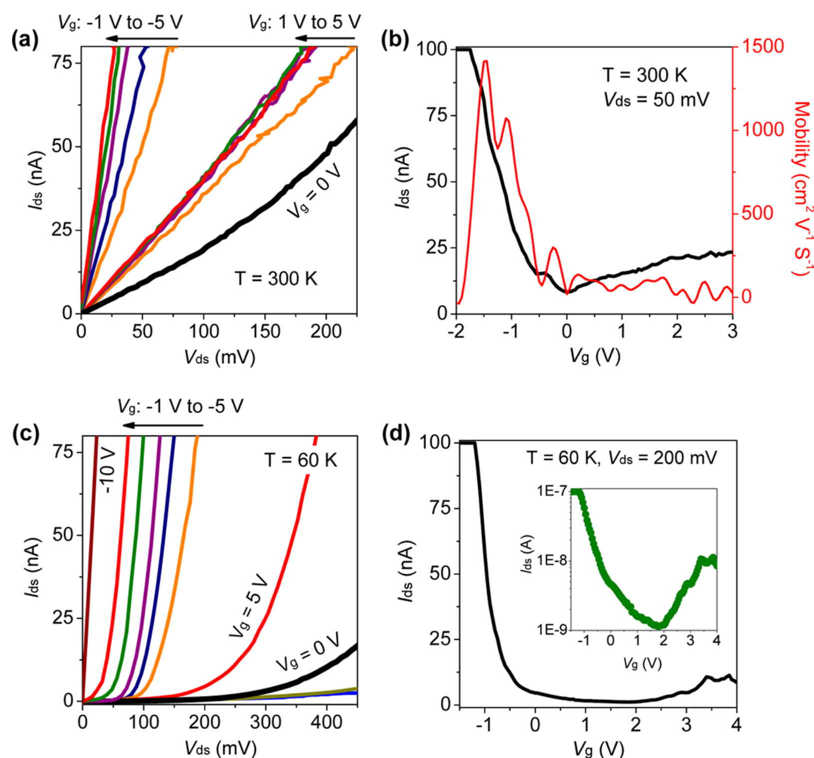

Figure 3. (a) Current−voltage ($I-V$) characteristics of a suspended nanotube device measured at room temperature. The $I-V$ curves show a linear feature and ambipolar transport behavior, indicating that the device is based on a small band gap SWNT. (b) Transfer characteristics of the suspended small band gap nanotube device, showing dependences of drain current (I_{ds}) and mobility on the gate voltage (V_g). Drain voltage (V_{ds}) bias is 50 mV. (c) $I-V$ and (d) transfer characteristics of the suspended small band gap nanotube device measured at 60 K. V_{ds} is biased at 200 mV.

thickness of the PMMA layer precoated on the Si/SiO_2 substrate. In this study, the height is 100 nm, and the nanotube channel length (L_{ch}) is 2 μm.[37]

The as-fabricated suspended nanotube devices were examined by electrical measurements performed in air or an Oxford cryostat. Both semiconducting and metallic SWNTs have been measured, which exhibit good performances comparable to the previous works (see Supporting Information, Figure S3),[12,14,26] indicating the high quality of the low-temperature deposited SWNTs. Very recently, Amer et al. compared the transfer characteristics of a metallic SWNT with its different segments suspended over or lying on the substrate, respectively.[9] The results indicate that the suspended segment possess a pronounced band gap due to the elimination of localized doping caused by trapped charges in the substrate, which is a general effect for all SWNTs. Therefore, we subsequently focus on the electrical properties of an as-fabricated device with a suspended small band gap SWNT. As shown in Figure 3a, the current−voltage ($I-V$) curve at zero gate bias is slightly nonlinear with a total resistance (R_{total}) of ∼6 MΩ, revealing the existence of a small Schottky barrier (SB) formed at the nanotube−metal contacts, which could be attributed to the pronounced band gap of the suspended nanotube. However, the SB can be effectively suppressed at both negative and positive gate voltage (V_g), leading to perfect linear $I-V$ characteristics. Meanwhile, R_{total} drops to ∼345 KΩ and ∼2.2 MΩ at $V_g = -5$ and 5 V, respectively. This ambipolar transport is an important feature for small band gap SWNTs.[7,11] Figure 3b plots the transfer characteristics of the device, revealing a prominent gate dependence. The corresponding field-effect mobility has also been calculated and plotted in Figure 3b by using the equation

$$\mu = \frac{L_{ch}}{V_{ds}C_g} g_m \quad (1)$$

where $L_{ch} = 2\ \mu$m is the nanotube channel length, $g_m = dI_{ds}/dV_g$ is the transconductance, and C_g is the gate capacitance per unit length of the SWNT, which can be calculated from

$$C_g = \left[C_q^{-1} + \frac{\ln(4T_{eox}/D)}{2\pi\varepsilon_0\varepsilon_{ox}} \right]^{-1} \quad (2)$$

where $C_q = 4 \times 10^{-10}$ F m^{-1} is the quantum capacitance of the nanotube,[38] $D = 1.6$ nm is the average diameter of SWNTs, ε_0 is vacuum permittivity, $\varepsilon_{ox} = 3.9$ is the relative dielectric constant of SiO_2, and $T_{eox} = 225.6$ nm is the effective dielectric thickness of the suspended device geometry, which is defined as[39]

$$T_{eox} = T_{ox} + \frac{\varepsilon_{air}}{\varepsilon_{ox}} T_{air} \quad (3)$$

where $T_{ox} = 200$ nm is the oxide thickness, $\varepsilon_{air} \approx 1$ is the relative dielectric constant of air, and $T_{air} = 100$ nm is the height of the suspended nanotube over the substrate. As shown in Figure 3b, the peak mobilities of the device are 1410 cm^2 V^{-1} S^{-1} for hole conduction (p channel) and 120 cm^2 V^{-1} S^{-1} for electron conduction (n channel), respectively. The p-channel mobility of the device is in the same order of magnitude as those of the CVD-grown SWNT devices reported in the previous works,[4,20] whereas both the conductance and mobility in the n channel are much lower. The asymmetric ambipolar transfer characteristics result from the asymmetric alignment between the Fermi level of the metal and the nanotube band structure. As previously mentioned, the band gap of a SWNT

becomes larger because of the suspended geometry. In our devices, the nanotubes contact with Au; because of its higher working function, the Fermi level will be aligned close to valence band of the nanotube.

Another feature in the transfer curve (Figure 3b) is the depleted current of 8.4 nA at $V_g^* = 0$ V. As previously discussed, a small but distinct SB is formed at nanotube−metal contacts and makes the $I-V$ curve at zero V_g slightly nonlinear. The nanotube band gap $E_g = \Phi_{Bp} + \Phi_{Bn}$, where Φ_{Bp} and Φ_{Bn} are SB heights for hole conduction and electron conduction, respectively. Apparently Φ_{Bp}, Φ_{Bn}, and E_g are comparable to $k_BT_{(300\text{ K})} \approx 26$ meV, where k_B is the Boltzmann constant and T is the temperature. Therefore, the thermally activated charge carriers can cross the SB even as the Fermi level is shifted within the band gap of the nanotube, which contributes a small background current, as measured in the transfer curve. This background current reaches its minimum value when the Fermi level is located at the middle of the band gap at $V_g^* = 0$ V, as measured in Figure 3b. This feature motivated us to investigate the temperature-dependent transport properties of this small band gap nanotube. Figure 3c shows the $I-V$ characteristics of the device at 60 K, which reveal a remarkable SB effect. Linear $I-V$ curves were measured only at a large negative gate $V_g = -10$ V. Figure 3d plots the corresponding transfer curve; it is expected that the depleted current decreases to 1.1 nA even at a larger V_{ds} bias.

Figure 4a shows the $I-V$ characteristics of the device measured at different temperatures down to 4 K at $V_g^* = 0$ V.

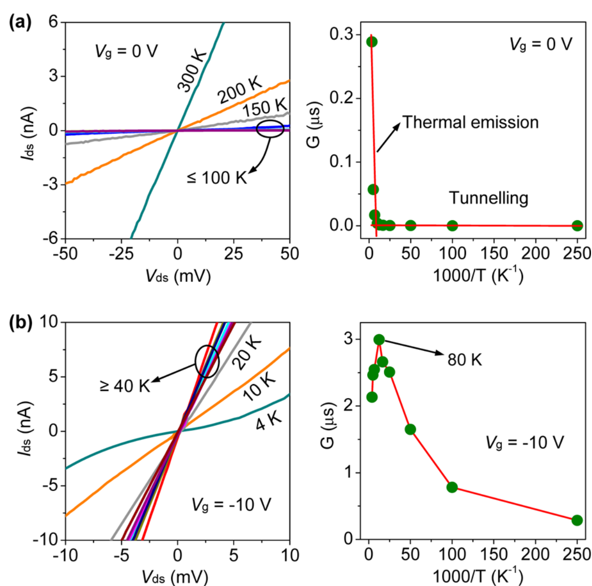

Figure 4. Temperature-dependent $I-V$ characteristics (left) and corresponding Arrhenius plot (right) at (a) $V_g = 0$ V and (b) $V_g = -10$ V, respectively. V_{ds} sweeps in a small range, and the zero bias conductance (G) is extracted for Arrhenius plotting. The corresponding standard deviation (SD) is found to be within 5% of the extracted G.

When the gate is biased near zero, the small I_{ds} is dominated by the thermally activated injection of charge carriers crossing the SB. Therefore, the measured current shows a sharp decrease from 300 to 100 K. At lower temperatures, however, the thermally activated conductance is suppressed and the carrier injection is dominated by tunnelling. The thermally activated conductance follows $G \propto \exp(-E_a/k_BT)$, and the corresponding thermal activation energy E_a can be extracted from the Arrhenius plot.[24] Here E_a is found to be ∼85 meV at $V_g^* = 0$ V; therefore, the band gap of the nanotube can be roughly estimated by $E_g = 2E_a = 170$ meV. While V_g is biased at −10 V, however, the temperature dependence of the $I-V$ characteristics exhibits very different features. As shown in Figure 4b, the measured current first shows a small variation, and sharp decrease only happens at temperatures lower than 40 K. The conductance increases from 2.1 to 3 μS from 300 to 80 K and then begins to decrease with further decreases in temperature, which is consistent with the previous results.[7] At $V_g = -10$ V, the Fermi level is shifted deeply into the valence band of the small-band gap SWNT, and thus the device shows quasi-metallic features. The conductance increase with $T > 80$ K can be attributed to the reduced phonon scattering as temperature decreases, whereas at lower temperature the effect of the small SB cannot be neglected any more (Figure 3c), and thus the conductance begins to decrease. The well-characterized temperature dependence of the device also indicates the cleanness and high quality of the suspended nanotube.

It is possible to gradually eliminate the contribution of thermal emission and uncover the tunnelling phenomena by decreasing the temperature. To detect the tunnelling transport at large negative gate, we applied a smaller $V_{ds} = 5$ mV and swept V_g from −8 V. As shown in Figure 5a, Fabry−Perot-like

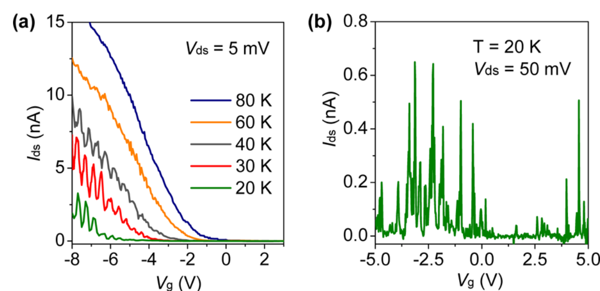

Figure 5. (a) $I-V_g$ characteristics of the suspended nanotube device recorded at $V_{ds} = 5$ mV under temperatures lower than 80 K. (b) Coulomb oscillations of the device at 20 K. To detect the oscillation peaks, the biased V_{ds} is increased to 50 mV.

bumps have been successfully measured with $T < 60$ K.[8,40] The interval between neighbor peaks $\Delta V_g = \sim 0.43$ V, independent of the slightly shifted peak positions at different temperatures. However, the conduction in small negative gate region and the n channel is undetectable at the applied small V_{ds}. We increase the V_{ds} to 50 mV, and Coloumb oscillation peaks have been detected (Figure 5b). These two different tunnelling features are determined by the V_g-induced specific alignments of the metal−nanotube band structure and also consistent with the temperature dependence of the nanotube conductance at different gate bias, as shown in Figure 4.

CONCLUSIONS

In conclusion, we have demonstrated a low-temperature and direct deposition of newly synthesized SWNTs via floating catalytic CVD. This approach can deposit SWNTs on various substrates and surfaces. A conventional process has further been developed to fabricate suspended nanotube devices based on this low-temperature deposition method. The quality of the nanotubes can be well-controlled, and the representative device with a suspended small band gap nanotube exhibits excellent transport characteristics at both room temperature and low

temperatures. These facilely fabricated suspended nanotube devices are promising for chemical/biosensing applications and also as single quantum dots or resonators. Moreover, the low-temperature deposition process is compatible with the current CMOS technology, which could enable further improvements on nanotube device fabrication.

■ ASSOCIATED CONTENT

Supporting Information

Raman spectrum of the SWNT thin films, optimization of the low-temperature SWNT deposition, and measurement data of more suspended nanotube devices. This material is available free of charge via the Internet at http://pubs.acs.org.

■ AUTHOR INFORMATION

Corresponding Author

*E-mail: zhaoyuanchun@hotmail.com (Y.Z.) and slf@nanoctr.cn (L.S.).

Notes

The authors declare no competing financial interest.

■ ACKNOWLEDGMENTS

This work was supported by National Science Foundation of China (grant nos. 10774032, 90921001).

■ REFERENCES

(1) Avouris, P.; Chen, Z.; Perebeinos, V. Carbon-Based Electronics. *Nat. Nanotechnol.* **2007**, *2*, 605−615.
(2) Wang, C.; Takei, K.; Takahashi, T.; Javey, A. Carbon Nanotube Electronics−Moving Forward. *Chem. Soc. Rev.* **2013**, *42*, 2592−2609.
(3) Franklin, A. D.; Luisier, M.; Han, S. J.; Tulevski, G.; Breslin, C. M.; Gignac, L.; Lundstrom, M. S.; Haensch, W. Sub-10 nm Carbon Nanotube Transistor. *Nano Lett.* **2011**, *12*, 758−762.
(4) Javey, A.; Guo, J.; Wang, Q.; Lundstrom, M.; Dai, H. Ballistic Carbon Nanotube Field-Effect Transistors. *Nature* **2003**, *424*, 654−657.
(5) Zhou, X. J.; Park, J. Y.; Huang, S. M.; Liu, J.; McEuen, P. L. Band Structure, Phonon Scattering, and the Performance Limit of Single-Walled Carbon Nanotube Transistors. *Phys. Rev. Lett.* **2005**, *95*, 146805.
(6) Zhang, Z. Y.; Wang, S.; Ding, L.; Liang, X. L.; Pei, T.; Shen, J.; Xu, H. L.; Chen, Q.; Cui, R. L.; Li, Y.; Peng, L. M. Self-Aligned Ballistic n-Type Single-Walled Carbon Nanotube Field-Effect Transistors with Adjustable Threshold Voltage. *Nano Lett.* **2008**, *8*, 3696−3701.
(7) Zhou, C. W.; Kong, J.; Dai, H. J. Intrinsic Electrical Properties of Individual Single-Walled Carbon Nanotubes with Small Band Gaps. *Phys. Rev. Lett.* **2000**, *84*, 5604−5607.
(8) Deshpande, V. V.; Chandra, B.; Caldwell, R.; Novikov, D. S.; Hone, J.; Bockrath, M. Mott insulating state in ultraclean carbon nanotubes. *Science* **2009**, *323*, 106−110.
(9) Amer, M. R.; Bushmaker, A.; Cronin, S. B. The Influence of Substrate in Determining the Band Gap of Metallic Carbon Nanotubes. *Nano Lett.* **2012**, *12*, 4843−4847.
(10) Liu, F.; Bao, M. Q.; Wang, K. L.; Liu, X. L.; Li, C.; Zhou, C. W. Determination of the Small Band Gap of Carbon Nanotubes Using the Ambipolar Random Telegraph Signal. *Nano Lett.* **2005**, *5*, 1333−1336.
(11) Wang, Z.; Ding, L.; Pei, T.; Zhang, Z.; Wang, S.; Yu, T.; Ye, X.; Peng, F.; Li, Y.; Peng, L. M. Large Signal Operation of Small Band-Gap Carbon Nanotube-Based Ambipolar Transistor: A High-Performance Frequency Doubler. *Nano Lett.* **2010**, *10*, 3648−3655.
(12) Javey, A.; Guo, J.; Farmer, D. B.; Wang, Q.; Wang, D.; Gordon, R. G.; Lundstrom, M.; Dai, H. Carbon Nanotube Field-Effect Transistors with Integrated Ohmic Contacts and High-κ Gate Dielectrics. *Nano Lett.* **2004**, *4*, 447−450.
(13) Kang, S. J.; Kocabas, C.; Ozel, T.; Shim, M.; Pimparkar, N.; Alam, M. A.; Rotkin, S. V.; Rogers, J. A. High-Performance Electronics Using Dense, Perfectly Aligned Arrays of Single-Walled Carbon Nanotubes. *Nat. Nanotechnol.* **2007**, *2*, 230−236.
(14) Franklin, A. D.; Chen, Z. H. Length Scaling of Carbon Nanotube Transistors. *Nat. Nanotechnol.* **2010**, *5*, 858−862.
(15) Cao, J.; Wang, Q.; Dai, H. J. Electron Transport in Very Clean, As-Grown Suspended Carbon Nanotubes. *Nat. Mater.* **2005**, *4*, 745−749.
(16) Sangwan, V. K.; Ballarotto, V. W.; Fuhrer, M. S.; Williams, E. D. Facile Fabrication of Suspended As-Grown Carbon Nanotube Devices. *Appl. Phys. Lett.* **2008**, *93*, 113112.
(17) Malapanis, A.; Jones, D. A.; Comfort, E.; Lee, J. U. Measuring Carbon Nanotube Band Gaps through Leakage Current and Excitonic Transitions of Nanotube Diodes. *Nano Lett.* **2010**, *11*, 1946−1951.
(18) Muoth, M.; Helbling, T.; Durrer, L.; Lee, S. W.; Roman, C.; Hierold, C. Hysteresis-Free Operation of Suspended Carbon Nanotube Transistors. *Nat. Nanotechnol.* **2010**, *5*, 589−592.
(19) Cao, J.; Wang, Q.; Wang, D.; Dai, H. Suspended Carbon Nanotube Quantum Wires with Two Gates. *Small* **2005**, *1*, 138−141.
(20) Pei, T.; Zhang, Z. Y.; Wang, Z. X.; Ding, L.; Wang, S.; Peng, L. M. Temperature Performance of Doping-Free Top-Gate CNT Field-Effect Transistors: Potential for Low- and High-Temperature Electronics. *Adv. Funct. Mater.* **2011**, *21*, 1843−1849.
(21) Wang, S.; Zeng, Q.; Yang, L.; Zhang, Z.; Wang, Z.; Pei, T.; Ding, L.; Liang, X.; Gao, M.; Li, Y.; Peng, L. M. High-Performance Carbon Nanotube Light-Emitting Diodes with Asymmetric Contacts. *Nano Lett.* **2011**, *11*, 23−29.
(22) Yang, L.; Wang, S.; Zeng, Q.; Zhang, Z.; Pei, T.; Li, Y.; Peng, L.-M. Efficient Photovoltage Multiplication in Carbon Nanotubes. *Nat. Photonics* **2011**, *5*, 673−677.
(23) Engel, M.; Steiner, M.; Sundaram, R. S.; Krupke, R.; Green, A. A.; Hersam, M. C.; Avouris, P. Spatially Resolved Electrostatic Potential and Photocurrent Generation in Carbon Nanotube Array Devices. *ACS Nano* **2012**, *6*, 7303−7310.
(24) Johnston, D. E.; Islam, M. F.; Yodh, A. G.; Johnson, A. T. Electronic Devices Based on Purified Carbon Nanotubes Grown by High-Pressure Decomposition of Carbon Monoxide. *Nat. Mater.* **2005**, *4*, 589−592.
(25) Wang, H.; Luo, J.; Robertson, A.; Ito, Y.; Yan, W.; Lang, V.; Zaka, M.; Schäffel, F.; Rümmeli, M. H.; Briggs, G. A. D.; Warner, J. H. High-Performance Field Effect Transistors from Solution Processed Carbon Nanotubes. *ACS Nano* **2010**, *4*, 6659−6664.
(26) Cao, Q.; Han, S. J.; Tulevski, G. S.; Franklin, A. D.; Haensch, W. Evaluation of Field-Effect Mobility and Contact Resistance of Transistors That Use Solution-Processed Single-Walled Carbon Nanotubes. *ACS Nano* **2012**, *6*, 6471−6477.
(27) Stokes, P.; Khondaker, S. I. High Quality Solution Processed Carbon Nanotube Transistors Assembled by Dielectrophoresis. *Appl. Phys. Lett.* **2010**, *96*, 083110−1−083110−3.
(28) Islam, M. R.; Kormondy, K. J.; Silbar, E.; Khondaker, S. I. A General Approach for High Yield Fabrication of CMOS-Compatible All-Semiconducting Carbon Nanotube Field Effect Transistors. *Nanotechnology* **2012**, *23*, 125201.
(29) Franklin, A. D.; Bojarczuk, N. A.; Copel, M. Consistently Low Subthreshold Swing in Carbon Nanotube Transistors Using Lanthanum Oxide. *Appl. Phys. Lett.* **2013**, *102*, 013108.
(30) Choi, S. J.; Bennett, P.; Takei, K.; Wang, C.; Lo, C. C.; Javey, A.; Bokor, J. Short-Channel Transistors Constructed with Solution-Processed Carbon Nanotubes. *ACS Nano* **2013**, *7*, 798−803.
(31) Ma, W. J.; Song, L.; Yang, R.; Zhang, T. H.; Zhao, Y. C.; Sun, L. F.; Ren, Y.; Liu, D. F.; Liu, L. F.; Shen, J.; Zhang, Z. X.; Xiang, Y. J.; Zhou, W. Y.; Xie, S. S. Directly Synthesized Strong, Highly Conducting, Transparent Single-Walled Carbon Nanotube Films. *Nano Lett.* **2007**, *7*, 2307−2311.
(32) Liu, Q. F.; Ren, W. C.; Chen, Z. G.; Wang, D. W.; Liu, B.; Yu, B.; Li, F.; Cong, H.; Cheng, H. M. Diameter-Selective Growth of Single-Walled Carbon Nanotubes with High Quality by Floating Catalyst Method. *ACS Nano* **2008**, *2*, 1722−1728.

(33) Zhou, W. Y.; Bai, X. D.; Wang, E. G.; Xie, S. S. Synthesis, Structure, and Properties of Single-Walled Carbon Nanotubes. *Adv. Mater.* **2009**, *21*, 4565−4583.
(34) Zhao, Y. C.; Song, L.; Deng, K.; Liu, Z.; Zhang, Z. X.; Yang, Y. L.; Wang, C.; Yang, H. F.; Jin, A. Z.; Luo, Q.; Gu, C. Z.; Xie, S. S.; Sun, L. F. Individual Water-Filled Single-Walled Carbon Nanotubes as Hydroelectric Power Converters. *Adv. Mater.* **2008**, *20*, 1772−1776.
(35) Dresselhaus, M. S.; Dresselhaus, G.; Saito, R.; Jorio, A. Raman Spectroscopy of Carbon Nanotubes. *Phys. Rep.* **2005**, *409*, 47−99.
(36) Kim, G. T.; Gu, G.; Waizmann, U.; Roth, S. Simple Method to Prepare Individual Suspended Nanofibers. *Appl. Phys. Lett.* **2002**, *80*, 1815−1817.
(37) Franklin, A. D.; Chen, Z. H. Length Scaling of Carbon Nanotube Transistors. *Nat. Nanotechnol.* **2010**, *5*, 858−862.
(38) Rosenblatt, S.; Yaish, Y.; Park, J.; Gore, J.; Sazonova, V.; McEuen, P. L. High Performance Electrolyte Gated Carbon Nanotube Transistors. *Nano Lett.* **2002**, *2*, 869−872.
(39) Wang, C.; Chien, J. C.; Takei, K.; Takahashi, T.; Nah, J.; Niknejad, A. M.; Javey, A. Extremely Bendable, High-Performance Integrated Circuits Using Semiconducting Carbon Nanotube Networks for Digital, Analog, and Radio-Frequency Applications. *Nano Lett.* **2012**, *12*, 1527−1533.
(40) Liang, W. J.; Bockrath, M.; Bozovic, D.; Hafner, J. H.; Tinkham, M.; Park, H. Fabry−Perot Interference in a Nanotube Electron Waveguide. *Nature* **2001**, *411*, 665−669.